Adaptive PI Control of the Hybrid Battery-Supercapacitor Storage in Standalone PV Power System

Ayman Alhejji
Department of Electrical Engineering, Yanbu Industrial College, Yanbu Industrial City, Saudi Arabia
alhejjia@rcjy.edu.sa (corresponding author)

Received: 3 February 2026 | Revised: 5 March 2026 | Accepted: 23 March 2026

 DOI: https://doi.org/10.48084/etasr.17945

ABSTRACT

This study explores how to improve the safety, reliability, and performance of off-grid Photovoltaic (PV) systems integrated with hybrid batteries and Supercapacitors (SCs) by using Adaptive Proportional-Integral (API) controllers. Adaptive hybrid power management is used to ensure the safety and continuity of the electricity supplied to the DC load and reduce voltage fluctuations owing to abnormal operation. The main contribution of this framework is the online API controller used in hybrid power management, which aims to protect the DC-link against damage and achieve faster performance and improved voltage stability of the power output of the generating system. The system architecture was simulated in MATLAB and included an off-grid PV system integrated with batteries and SCs to maintain a stable DC load. The results of the simulation show that the DC-link voltage instability is improved by the API controller compared to the fixed PI controller, which is fine-tuned by various optimization techniques in the case of sudden environmental and load changes.

Keywords-PI; DC-DC boost converter; DC-DC bidirectional converter; hybrid battery-supercapacitor; energy management

I. INTRODUCTION

For off-grid Photovoltaic (PV) power systems, the intermittent nature of solar energy poses a challenge, making the integration of energy storage systems imperative. Energy storage systems are considered the backbone of off-grid PV power systems. Integrating a battery bank into an off-grid PV power system ensures the continuity of power flow to the load. However, the unpredictable behavior of batteries and their struggle to deliver quick energy pose challenges. Nevertheless, the capability of energy storage systems may be harmed by the restricted lifetime of batteries caused by intermittent power usage and variable power sources. To increase the number of charge and discharge cycles in these systems, different energy storage technologies are being investigated. For example, Supercapacitors (SCs), flywheels, hydroelectric power plants, compressed air energy storage, and other devices are among them [1, 2]. Therefore, a SC is incorporated into grid-off PV power systems to reduce the stress on the battery by accounting for transient load conditions and complementing battery deficiency [3]. Authors in [4, 5] focused on SCs, also known as ultracapacitors or electrical double-layer capacitors, which offer several advantages, such as high-power density, long cycle life, high efficiency, wide temperature range, and environmental friendliness compared to traditional batteries and capacitors. SCs, which have a high power density, are necessary for applications like electric vehicles and renewable energy systems to guarantee power continuity and stability, as well as to smooth out power fluctuations. SCs are often combined in a hybrid energy storage system to produce a more effective and adaptable energy storage solution that boosts performance, prolongs battery life, enhances safety, reduces the cost of batteries and maintenance, and buffers fluctuating power demand [6, 7]. Although batteries have a higher energy density, which allows for long-term energy storage, SCs are distinguished by their capacity to instantly provide and recuperate energy at high power. A hybrid energy storage system can achieve an ideal equilibrium between high power and high energy storage capacity. The SCs are incorporated with batteries to reduce reliance on traditional batteries and the negative environmental effects of battery waste.

Hybrid SCs are devices that combine a battery-like electrode with a capacitive electrode that can act as either an anode or a cathode [8]. These SCs can be divided into three distinct groups according to the electrode sorting: asymmetric hybrids, battery-type hybrids, and compound hybrids [9]. Authors in [10] studied energy storage system types, uses, comparisons, and recent advances, in response to the literature's reports on various control systems for hybrid energy storage systems of battery and SC consolidation. Table I summarizes the comparative characteristics of the DC link voltage controllers used in other studies.

Literature on DC-link voltage control shows a variety of approaches to regulate the charging and discharge of energy storage, and thus reduce the DC-link voltage fluctuations [11-

16]. For instance, fuzzy logic control has been employed to redistribute the demand between battery and SC hybrid energy storage according to their state of charge, and so protect them from overcharging and deep discharge [11]. As reported in [12], the independent current controllers in both the battery and SC DC-DC converters provide appropriate charge and discharge. The SC's current controller fine-tunes its parameters, resulting in faster reaction than a battery. Moreover, a Firefly algorithm with particle swarm optimization was used to reduce the DC link voltage fluctuations of electric vehicles [13]. An adaptive filter-based method, presented in [14], was employed in hybrid energy storage to reduce DC-link voltage spikes by allocating the charging and discharging currents for each storage device within the DC microgrid according to its charging status. Another control method was proposed in [15], which employed a feedback/feedforward control strategy in a battery energy storage system to reduce the DC link voltage fluctuations with reduced DC link capacitance volume and cost. In addition, another solution was presented in [16], which reduces the DC-link voltage fluctuations using a feedforward controller. In [17], a control strategy was proposed using distributed charge and discharge control of the DC link in renewable energy coupled with energy storage.

Power Management System (PMS) has been utilized for optimally managing the power flow that circulates between the inputs and outputs of the system [18-25]. Authors in [18] addressed inherent control for an energy management system of a grid-connected PV coupled with a battery to enable the system to function as a distributed source within the utility grid. Another solution was presented in [19], in which the power management was capable of meeting the multi-objectives of an off-grid PV-battery system, ensuring that there was no overcharging, no energy transferred to the dump load, and no excess power output. In [20], a model predictive control in PMS for a microgrid-integrated PV-battery energy system for voltage stabilization and power balancing in buildings was presented. In [21], a model predictive power management was employed for PVs merged with a hybrid battery SC to enhance system reliability by predicting load demand using the support vector machine. In [22], the designed energy management was based on variable-gain-enhanced second-order generalized integrator frequency-locked loop controls, which enhanced the system performance and reduced the operating costs. In [23], an adaptive frequency-based control with state of charge management was performed to guarantee smooth operation. Moreover, a self-adaptive bonobo optimization-based fractional order Proportional-Integral (PI) controller was employed in [24] to manage and control the battery/SC simultaneously. Similarly, in [25], a control strategy was employed to ensure power distribution between the hybrid battery and SC, while simultaneously decoupling low- and high-frequency current components and regulating the state-of-charge within specified limits.

This study addresses these research gaps by developing and validating an Adaptive Proportional-Integral (API) controller for DC link voltage regulation in an off-grid PV system integrated with hybrid battery–SC storage. Unlike earlier studies, the proposed API aims to:

1. Ensure robust voltage stability under nonlinear solar irradiance and load variation.
2. Facilitate power sharing between the battery and SC, thereby reducing battery stress and extending lifetime.
3. Provide a simple adaptive control mechanism.

TABLE I. DESCRIPTION OF PREVIOUS RELATED WORKS ON DC-LINK VOLTAGE CONTROL

System	Controller type	Adaptation strategy	Key outcomes	Limitations
Grid-tied inverter [1]	Adaptive PI	Online tuning of K_p, K_i	Fast transient, low ripple, reduced THD	Limited to small-signal stability, not tested under storage dynamics
Single-phase PV inverter [2]	Adaptive PI	Adaptive gain scheduling	Balanced ripple and harmonic reduction	Focused only on single-phase, no hybrid storage
PV boost converter [3]	Adaptive PID (PI core)	Plant parameter adaptation	Maintains DC-link despite irradiance change	Complexity increases for multi-source hybrid
General DC-link controllers [4]	PI (review)	Design guidelines	Framework for DC-link PI tuning	Not adaptive in implementation (reference only)
Wind DFIG system [5]	Self-tuning PI	Neural adaptation	Robust to parameter shifts	Not hybrid storage focused
Isolated microgrid [6]	Adaptive PI	Bayesian adaptive laws	Improved stability and optimal operation	Heavy computational demand
Boost converter w/ CPL [7]	PI + adaptive	Passivity-based gain update	Stabilizes under CPL disturbance	Controller complexity
Tramway DC-bus [8]	Adaptive PI	SoC-aware PI	Reduced 77% transient peak	Limited to transport applications
HVDC systems [9]	Optimized PI	Offline optimization	Stability under HVDC faults	Not adaptive; no hybrid E-storage
DC microgrid bus [10]	Hybrid PI	Cascade + backstepping	Robust DC-bus voltage	Difficult to implement in real-time
DC microgrid [11]	Adaptive PI	Model-reference adaptation	Stable DC-bus under load	Lack of hybrid PV-batt-SC testing

Variations in solar irradiance and temperature may affect the performance of Maximum Power Point Tracking (MPPT) and require control methods that are adaptive. Thus, API control is proposed to control DC link voltage variation and contribute to the control of PWM of the boost converter, and simultaneously control the energy management of the DC-DC bidirectional converters of the battery and SC units. The bidirectional converter can perform a variety of tasks, including simultaneous energy storage and release, as well as increasing battery utilization to provide a steady output. Above all, the DC-DC bidirectional converters may enhance system stability by stabilizing the DC link voltage and lowering voltage

variation when the API controller is used. The API is therefore capable of providing smooth and fast power sharing and stability of the off-grid PV system with hybrid battery SC energy storage compared with that of an optimized PI controller based on the Genetic Algorithm (GA) and Lightning Attachment Procedure Optimization (LAPO) techniques.

II. CONFIGURATION OF THE STUDIED SYSTEM

A. *Solar Photovoltaic Model*

In this article's framework, the solar PV module is depicted in Figure 1 [24] as a current source with diode, series, and shunt resistances [26], and the PV system's V-I characteristics are shown in Figure 2.

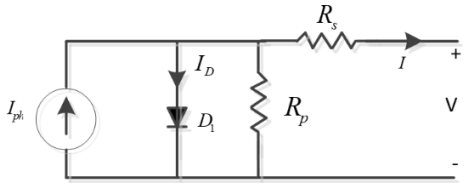

Fig. 1. A solar cell equivalent circuit [24].

The current is expressed as:

$$I = n_p I_{ph} - n_p I_s \left[\exp\left(\frac{V+I.R_s\left(\frac{n_m}{n_p}\right)}{V_T}\right) - 1\right] - \left[\frac{V+I.R_s\left(\frac{n_m}{n_p}\right)}{R_p\left(\frac{n_m}{n_p}\right)}\right] \quad (1)$$

where I and V are the output current and voltage of the PV panel, respectively. Furthermore, I_{ph} is the photo-current, I_s describes the cell saturation of dark current, and n_m and n_p are the numbers of PV cells connected in series and parallel, respectively. In addition, R_s and R_p define the resistance in series and parallel, respectively. $V_T = n_s kT/q$ is the thermal voltage of the PV module in volts, while k=1.3805×10^{-23} J/K is Boltzmann's constant, and q=1.60217646×10^{-19} C is the electron charge.

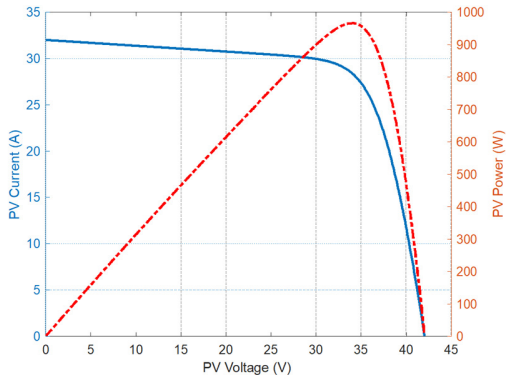

Fig. 2. V-I and P-V characteristic profiles of a solar PV array.

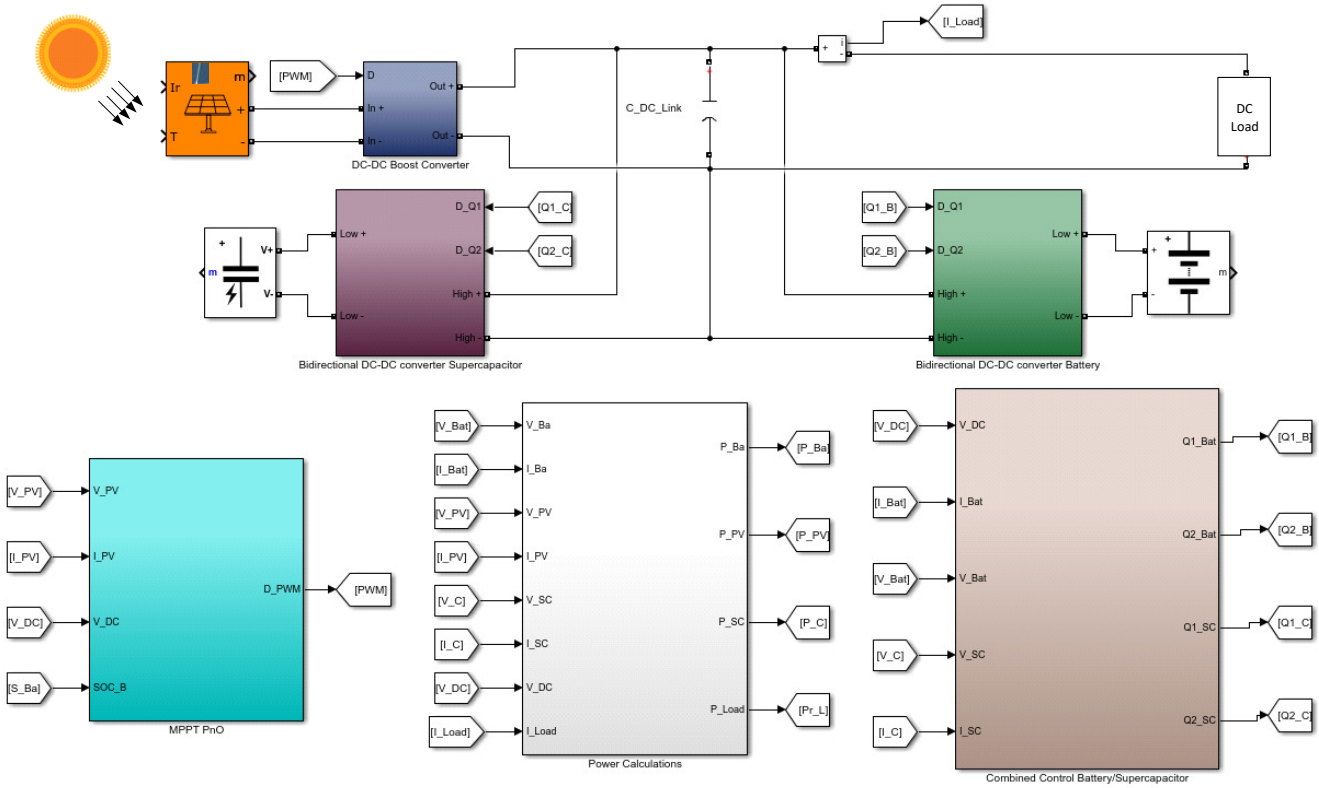

Fig. 3. Control framework of off-grid solar PV integrated with a hybrid battery-SC energy system.

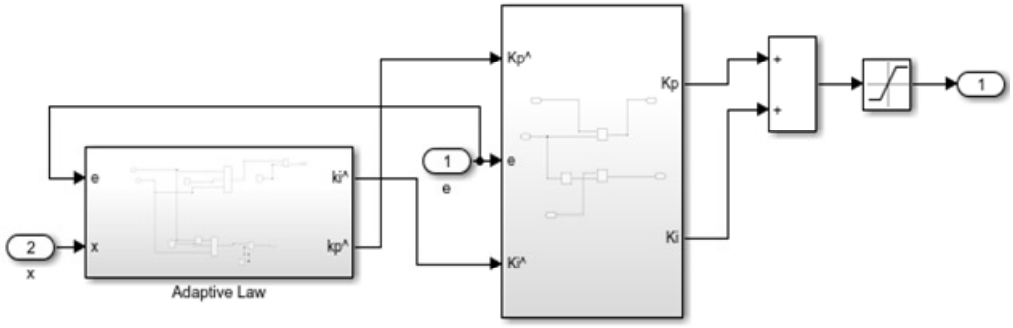

Fig. 4. API controller scheme.

Figure 3 displays the proposed off-grid solar PV system that is being investigated. It comprises a DC-DC boost converter that connects a solar PV system to the DC bus. In this scheme, the SC and battery form the hybrid energy storage unit. A DC-DC boost converter is mainly connected to the solar PV panel on one side and the DC link on the other side. This DC link also connects the DC-DC bidirectional converters to their respective energy storage. The advantage of this DC link is to maintain the balance and system stability between the source and load, and ensure stable energy sharing while storing and supplying.

The solar PV panel is used as the primary source, the battery immediately operates when there is an excess or shortage of power supply, and the SC is utilized to effectively minimize the variance of either the PV or the load. These three sources are employed to increase the reliability of delivered power to a DC load. A PI controller is utilized to stabilize the output voltage of each DC-DC buck-boost converter by producing a proper PWM. The MPPT is utilized to extract the maximum power from the solar PV panel to drive the DC-DC boost converter and DC power transfer, and potent power management is employed to govern the entire system [27].

The total power expression in the overall system is described as:

$$P_{pv} - P_{sc} - P_{batt} - P_{load} = 0 \quad (2)$$

where P_{pv} is the PV power in W, P_{sc} describes the power flow of the SC after power conversion, P_{batt} is the power flow of the battery, and P_{load} represents the load demand.

B. PWM of DC-DC Boost Converter

As shown in Figure 3, in MATLAB/SIMULINK, the DC/DC converter connected to the PV system depends on different inputs, such as the MPPT, battery status, and DC-link voltage, to enhance the performance of the PV power-generation system and generate PWM based on the API controller portrayed in Figure 4 and the classic controller presented in [27]. These inputs were operated according to the flowchart algorithm displayed in Figure 5. However, other coupling batteries with SCs can fully utilize their respective advantages and enhance the performance of hybrid energy storage. Table II summarizes the component specifications of the DC-DC boost converter controlled by MPPT in this study.

TABLE II. SPECIFICATIONS OF THE DC-DC BOOST CONVERTER

Parameter	Value
Diode resistance, R_{on}	0.0001 Ω
Inductor, L	0.352 mH
Capacitor, C	2200 µF
Switching frequency	5 kHz

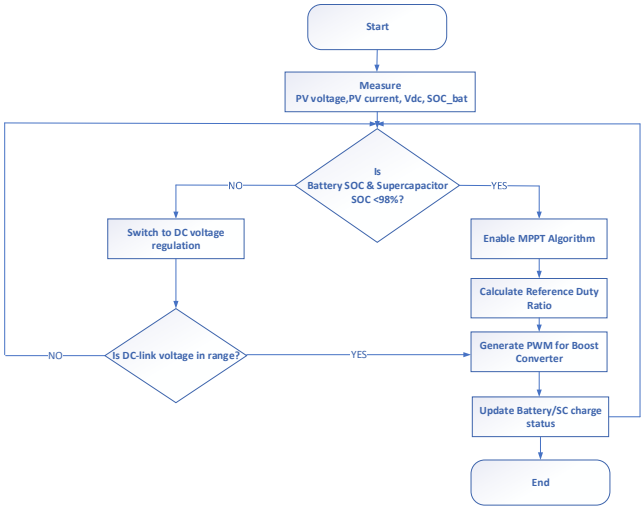

Fig. 5. Flowchart of the PWM control strategy for the DC-DC boost converter.

C. Battery

Typically, the equivalent circuit of the battery comprises an internal resistance and terminal voltage, either connected to a load or considered open circuit voltage. It functions as a substantial power source, even in off-grid PV systems. Figure 6 illustrates the charging and discharging control scheme. As shown in Figure 7, a DC/DC converter connects the batteries of an off-grid PV system to a DC link such that the voltage of the battery and the DC link are equivalent, as given in [28].

The current of the battery has a specific range for safety reasons:

$$I_{bat,min} \leq I_{bat} \leq I_{bat,max} \quad (3)$$

The State of Charge (SoC) of the battery is expressed as:

$$SoC_{bat} = SoC_0 - \frac{1}{Q}\int_0^t I_{bat}\, dt \quad (4)$$

where SoC_0 is the initial value of the SoC, Q is the capacity of the battery, and I_{bat} is the current delivered through the battery. This current is positive only during feeding the load demand and negative during charging. To observe the SoC of the battery, the SoC must be maintained within a specific range to increase system stability and safety, and is expressed as:

$$SoC_{bat,min} \leq SoC_{bat} \leq SoC_{bat,max} \quad (5)$$

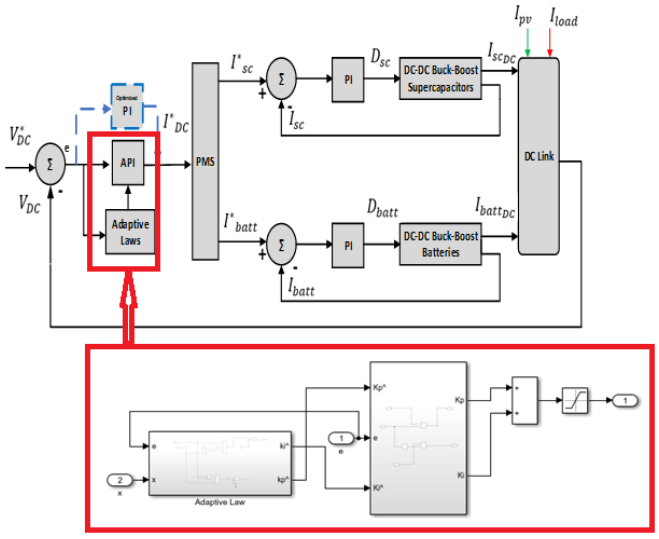

Fig. 6. Control diagram for power management with the battery and SC converters.

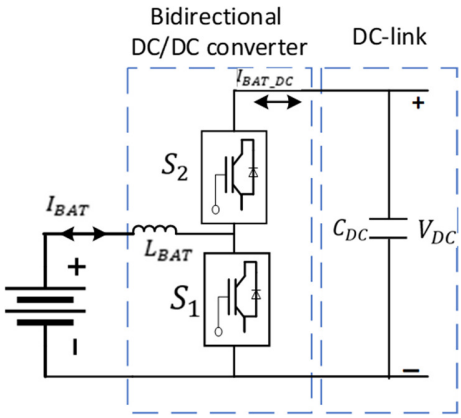

Fig. 7. Battery configuration with a bidirectional DC-DC converter.

D. Supercapacitor

SCs, also known as ultra-capacitors or double-layer capacitors, have a high capacity of over a thousand Farads despite their low voltage of 2.7 V [8, 26]. SCs differ from ceramic or electrolytic capacitors in that they lack a dielectric between the positive and negative electrodes. It exploits the Electrical Double Layer (EDL) that forms at the interface of the solid electrode and liquid electrolyte rather than filling the space between the two electrodes with an electrolyte that contains both positive and negative ions.

As shown in Figure 8, the SC connected to a bidirectional (bulk/boost) converter consists of a straightforward two-resistor RC circuit. The equivalent series resistance, R_s, is the resistance in series with the capacitor, whereas the equivalent parallel resistance, R_p, is the resistance in parallel with it [26]. The self-discharge phenomenon of an ultracapacitor when it is operating under no-load conditions is represented by the parallel resistance, R_p. Usually, the series resistance causes a sharp decrease in voltage at the end of the charging cycle and a sharp increase in voltage at the end of the discharging cycle. The mathematical expression of the SC current is given by [23]:

$$I_{sc} = \frac{U_{sc}SoC - \sqrt{(U_{sc}SoC)^2 - 4P_{sc}R_{sc}}}{2R_{sc}} \quad (6)$$

The power of the SC in W is described as:

$$P_{sc} = U_{sc}I_{sc} - I_{sc}^2 R_{sc} \quad (7)$$

To keep the power of the SC within a certain range, it is enforced as:

$$P_{sc-min} \leq P_{sc} \leq P_{sc-max} \quad (8)$$

The SoC of the SC can be obtained from the following expression based on the maximum and minimum voltages of the SC:

$$SoC_{sc} = \frac{U_{sc} - U_{sc-min}}{U_{sc-max} - U_{sc-min}} \quad (9)$$

To observe the SoC of the SC, the SoC must be kept within a specific range to increase the system stability and safety, as:

$$SoC_{sc,min} \leq SoC_{sc} \leq SoC_{sc,max} \quad (10)$$

SoC control was used to prevent overcharging/overdischarging and repeated changes in the energy storage unit.

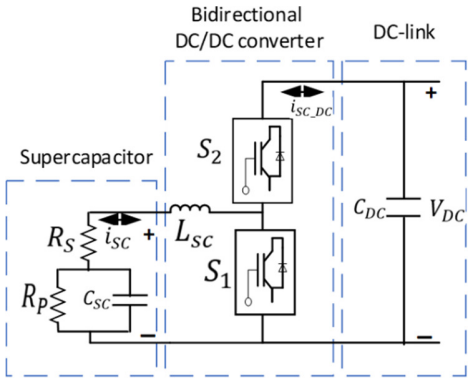

Fig. 8. SC configuration with a bidirectional DC-DC converter.

III. CONTROL STRATEGY

This section provides details for two different types of controllers employed to regulate the DC-link voltage and protect the hybrid energy storage system, as shown in Figure 6 and discussed below.

In a typical control PMS, a fixed PI controller is employed to control the flow from the generated solar PV power, load, and energy storage between the hybrid battery SC unit

described in [29]. However, this type of fixed controller has several problems, the most important of which are the need for tuning, the linear control type, and slow dynamics. For this reason, API control is proposed to handle the power control management system in this framework.

By integrating battery SC hybrid energy storage into the off-grid PV system managed by a smart power management system, the load energy consumption can be easily predicted [21].

Table III summarizes the component specifications of the bidirectional converter for both the battery and SC. In addition, the bidirectional DC-DC converter dynamics of both the battery and SC are formulated as:

$$\left.\begin{aligned} \frac{di_{L,bat}}{dt} &= \frac{1}{L_{bat}}(d_{bat}V_{bat} - V_{dc}) \\ \frac{di_{L,sc}}{dt} &= \frac{1}{L_{sc}}(d_{sc}V_{sc} - V_{dc}) \\ \frac{dV_{dc}}{dt} &= \frac{1}{C_{dc}}(i_{L,bat} + i_{L,sc} - \frac{V_{dc}}{R_{load}}) \end{aligned}\right\} \quad (11)$$

where $i_{L,bat}$ and $i_{L,sc}$ are the battery current variable and SC current variable, respectively. L_{bat} and L_{sc} are the battery inductance and SC inductance in Henry, respectively. Moreover, C_{dc} represents the DC-link capacitance in Farads. R_{load} is the load demand.

The duty cycles of both the battery and SC converters to maintain the DC-link voltage at the level of the DC-link voltage reference are:

$$D_{batt} = sat(K_P e_{bat} + K_I \int e_{bat} \ dt) \quad (12)$$

$$D_{sc} = sat(K_P e_{sc} + K_I \int e_{sc} \ dt) \quad (13)$$

where D_{batt} and D_{sc} describe the duty cycles of the battery converter and SC converter, respectively.

For the current sharing strategy, the SoC determines the currents of the hybrid battery SC energy storage as:

$$I^*_{batt} = (1 - \gamma(t))I^*_{DC} \quad (14)$$

$$I^*_{sc} = \gamma(t)I^*_{DC} \quad (15)$$

where $\gamma(t)$ is dependent on the SoC and can be modified to regulate the current references. In addition, I^*_{DC} describes the DC-link current reference to update the PMS. Figure 6 illustrates the replacement of the fixed PI/optimized PI controller with the API controller. Their comparison is shown in the simulation and results.

The power-sharing crossover point is implemented inside the control architecture; hence, the separation is deliberately designed by a filtering mechanism. The fixed-gain PI or API controller is activated based on the error dynamics of the DC link voltage. The fixed-gain PI or API controller output provides the overall compensation power, after which the frequency separation block allocates power between the battery and the SC.

TABLE III. SPECIFICATIONS OF THE DC-DC BIDIRECTIONAL CONVERTER

Parameter	Value
Inductor L_{sc} and inductor L_{BAT}	0.355e-3 H
Capacitor C_{DC}	300e-6
Switching frequency	16 kHz
Resistor	0.05 Ω
Internal resistor R_{on}	1e-3
Snubber resistor R_s	1e5
Snubber capacitance	Infinite

A. Optimized PI Controller

When operating conditions change, the DC link voltage V_{DC} changes rather than the reference DC voltage (V^*_{DC}) of 50 V. This change affects the output power, current, and voltage. When this DC link voltage is properly regulated, system performance is enhanced. The PI controllers with fixed gains K_p and K_i are determined by the GA [30-32] and LAPO techniques [33-35] in order to regulate the DC-link voltage. For determining the PI control parameters, the optimization techniques minimize the error in the objective function, given as:

$$J = \int_0^t (V^*_{DC} - V_{DC})^2 \ dt \quad (16)$$

1) Genetic Algorithm

The GA is a mature optimizer in which the fitted genes or individuals are chosen for reproduction [30, 32]. The GA optimization is aimed at determining the optimal gains of the PI controller, and the following steps are included in the GA guidelines:

1. The algorithm randomly starts reading the objective function (16), and then an initial population (POP_0) is assumed.

2. The constraints in (POP_0) are verified. The solutions that are outside the constraints are eliminated with a large penalty.

3. The objective function (J) is checked and evaluated at (POP_0), and a new solution is generated (POP_k).

4. Another population is generated (POP_{k+1}) via GA elitism, selection, crossover, and mutation.

5. The constraints are checked for a solution (POP_{k+1}). The simulation is stopped for a previously determined number of iterations. Ultimately, the best solution is printed.

2) Lighting Attachment Procedure Optimization

The lightning attachment mechanism is a physical phenomenon that serves as the basis for the LAPO algorithm, which is a heuristic optimization technique. A flash is generated when the massive electrical load stored in the clouds increases. As a result, the electrical strength increases. In contrast to previous population-based methods, the process of optimizing the LAPO algorithm, as shown in Figure 9, is divided into two main phases: the spread of the upward leader and the movement of the downward leaders. The lightning process stops when the upward and downward leaders come into contact with each other, and the striking place is determined. The optimization process is always completed when the convergence criteria are met. To improve

performance, this method calculates the population average after each iteration and then evaluates the fitness of the average solution. If the fitness of the worst solution is lower than that of the average solution, the average reaction is used, as provided in [33]. This LAPO was improved and used in [34] to determine the optimal reactive power under uncertainties of renewable generation. The LAPO was a solution for achieving the Low Voltage Ride-Through (LVRT) in addition to the fuzzy controller integrated with PV and wind power [35].

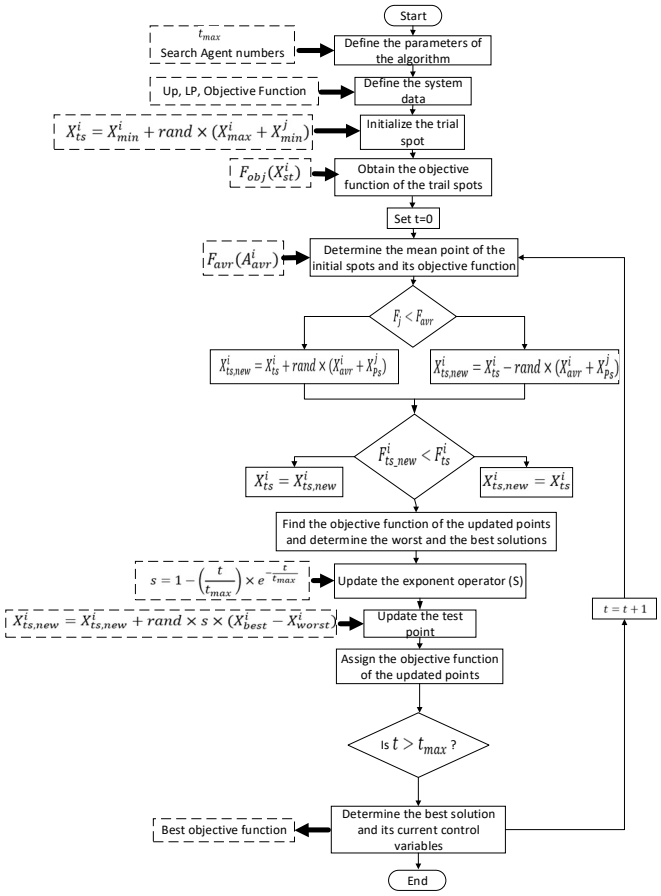

Fig. 9. LAPO flowchart [33].

B. Adaptive PI Control

The proposed API controller effectively addresses the constraints of fixed-gain PI controllers within complex, nonlinear, and time-varying off-grid PV hybrid systems. Conventional PI controllers exhibit challenges such as sensitivity to gain, suboptimal transient response during variations in irradiance and load, issues with integral windup, and diminished robustness in the face of changes in battery parameters. The adaptive mechanism implements online adjustments to the proportional and integral gains in response to the dynamics of DC-link voltage error. By enhancing the gains during significant disturbances and reducing them during stable operation, the API facilitates a quicker transient response, minimizes voltage overshoot, improves power-sharing precision between the battery and SC, and strengthens overall system robustness.

The developed API controller was inserted in place of the fixed-gain PI controller. The error signal of the DC voltage regulator represents the difference between the voltage reference V_{DC*} and the measured voltage V_{DC}. Such signal controlled by the API controller can adjust its parameters and then generate the desired current for the PMS, as shown in Figure 5. Subsequently, another error signal between the current reference and actual value is driven by the fixed-gain PI current controller, which accurately determines the duty cycles of each converter, as depicted in Figure 6. Then, this controlled duty cycle is fed into the DC-DC converter to act either in boost or bulk mode as being a DC-DC bidirectional converter connected to the battery and SC. This control strategy can guarantee an enhanced battery lifespan.

The error in the DC link voltage is described by:

$$e = V_{DC}^* - V_{DC} \tag{17}$$

The generated reference DC current based on the optimized PI, as shown in Figure 6, is formulated as:

$$I_{DC}^* = K_P e + K_I \int e\, dt \tag{18}$$

Moreover, the generated reference DC current based on the API controller, shown in Figure 6 and formulated in (18), is:

$$I_{DC}^* = \hat{K}_P e + \hat{K}_I \int e\, dt \tag{19}$$

where the adaptive control parameters are adjusted based on subsequent adaptation rules, designed and analyzed by [36], as:

$$\dot{\hat{K}}_P = \Gamma_1 \times \frac{|V_{DC}^* - V_{DC}|}{|V_{DC}^* - V_{DC}| + 1} \tag{20}$$

$$\dot{\hat{K}}_I = \Gamma_2 \int \frac{|V_{DC}^* - V_{DC}|}{|V_{DC}^* - V_{DC}| + 1} \tag{21}$$

where Γ_1 and Γ_2 are the adaptation gains for adaptive laws.

IV. RESULTS AND DISCUSSION

The proposed API controller was used to enhance the energy management of standalone PV power generation integrated with hybrid energy storage compared with that of the optimized PI controller. This API controller, activated based on the error dynamics of the DC-link voltage, designed in DC-DC bidirectional converters, controls and enhances the power management performance in terms of the power sharing among the battery and SC to ensure the stable operation of the standalone PV power system. Furthermore, the API controller is compared with the optimized PI controller to demonstrate the effectiveness of the proposed controller. The simulation performance results were obtained using MATLAB R2022b under different operating scenarios. Table IV details all the component specifications of the off-grid solar PV plant along with the hybrid energy storage capacity for this study.

Table V describes the different control characteristics employed in this study, where three controllers, API, GA-PI, and LAPO-PI, are used for the best control of the DC-link voltage, and Integral of Time Absolute Error (ITAE) is utilized as a performance metric.

TABLE IV. SPECIFICATIONS OF THE OFF-GRID SOLAR PV PLANT AND DC-DC BOOST CONVERTER

Parameters	Values
Irradiance	200-1000 W/m^2
Open-circuit voltage V_{oc}	21 V
Voltage at maximum power V_{mp}	17 V
Short-circuit current I_{sc}	8 A
Current at maximum power I_{mp}	7.1 A
Maximum power at STC W_p	120.7 W
DC input voltage V_{in}	11 V
Output capacitor C_0	300 µF
DC output voltage	50 V
DC link voltage reference	50 V
SC parameter	32 V, 29 F
Lithium-ion battery parameter	24 V, 14 Ah

TABLE V. TYPICAL SIMULATION RESULTS

Controller	Type	Controller flexibility	Strength
API	Rule-based online adaptation	Online adjustment of controller	Fast dynamic adaptability
GA-PI	Offline optimization	Fixed controller minimizes the ITAE	Balanced steady-state accuracy
LAPO-PI	Offline optimization	Fixed controller minimizes the ITAE	High robustness and convergence reliability

A. Solar Irradiance and Temperature Variations

The variations in solar irradiance and temperature are inevitable; however, it is significant to reduce the impact of such variations, especially in off-grid PV systems. Therefore, SCs and batteries are integrated into the system as hybrid energy storage devices to ensure continuity despite weather variations. When the solar irradiance and temperature vary, as shown in Figure 10, the DC-link stability is affected. Therefore, an API was proposed to stabilize the DC link and recover the voltage with less overshoot.

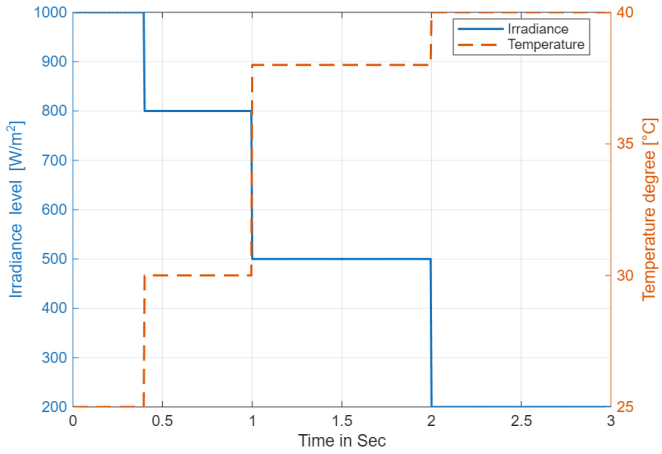

Fig. 10. Solar irradiance and temperature profiles.

In this study, an API controller was applied to control the DC link and improve performance. The PV power directly changes according to the irradiance changes, as illustrated in Figure 11.

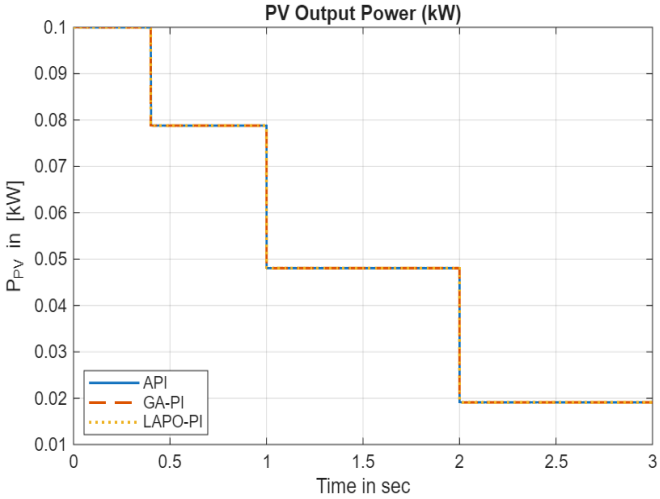

Fig. 11. PV power output under solar irradiance and temperature variations.

Under irradiance and temperature variations of different instants, such as 0.75 s, 1.5 s, and 2.25 s, the dynamic performance of the DC-link voltage using three controllers, namely adaptive PI, GA-based PI, and LAPO-based PI, is displayed in Figure 12. The voltage amplitude of the DC link varied, was slightly reduced, and then recovered to its reference value of 50 V. The DC-link voltage was less affected by the different irradiance levels when the API controller was employed. Moreover, it ensures fast response with less overshoot and maintains the DC-link voltage by achieving acceptable steady-state accuracy over other optimized PI controllers used.

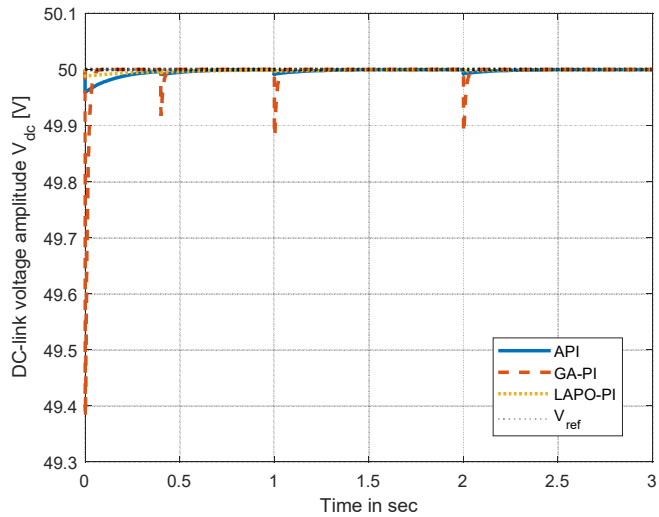

Fig. 12. DC link voltage performance.

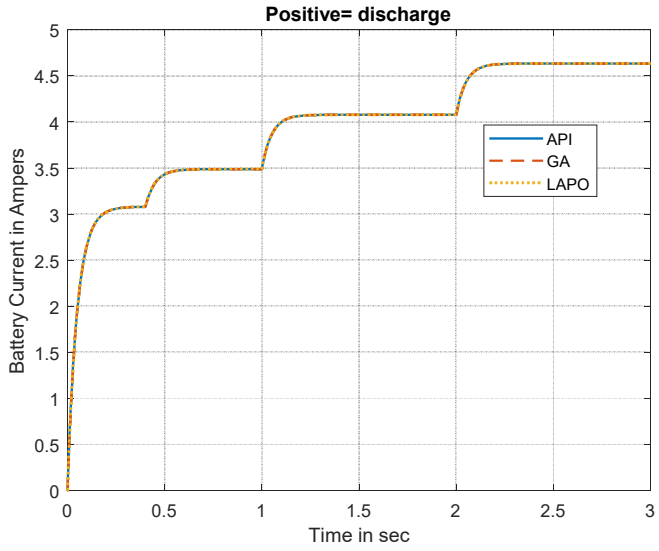

Fig. 13. Battery current.

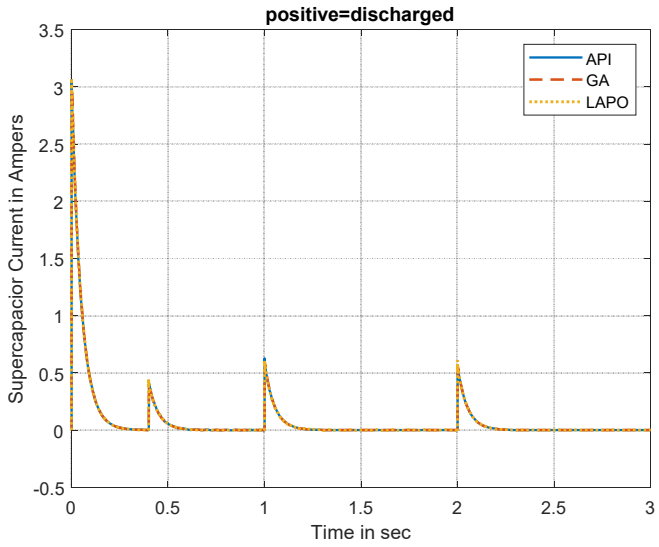

Fig. 14. SC current.

The battery current, as depicted in Figure 13, corroborates that the suggested API controller facilitates seamless and steady current distribution by enabling the battery to provide only the average power requirement. This reduces the current ripple and overshoot, thereby alleviating battery stress and improving the longevity and reliability of the off-grid PV system. However, the current response of the SC, shown in Figure 14, confirms its function as a compensation for transient power in the hybrid energy storage system. Therefore, the battery is protected from high-frequency stress, and DC-link voltage fluctuations are efficiently suppressed by rapid, high-magnitude current exchange. By guaranteeing rapid damping and steady current coordination under dynamic operating conditions, the API controller enhances this behavior by ensuring prompt damping.

The battery-SC power performance, as demonstrated in Figure 15, during solar irradiance and temperature change is evident, where the SC handled the transient at 0.4 s, and the battery power increased. The power of the battery, as shown in Figure 15, increased once the PV power started to decrease owing to low irradiance (400 W/m^2) at 0.4 s, and simultaneously, the SC power was quickly supplied and handled the transient to aid the battery during this PV power reduction. When the irradiance increased at 1 s, the PV power increased, and the battery and SC started discharging power slowly and then charged in a stable operation.

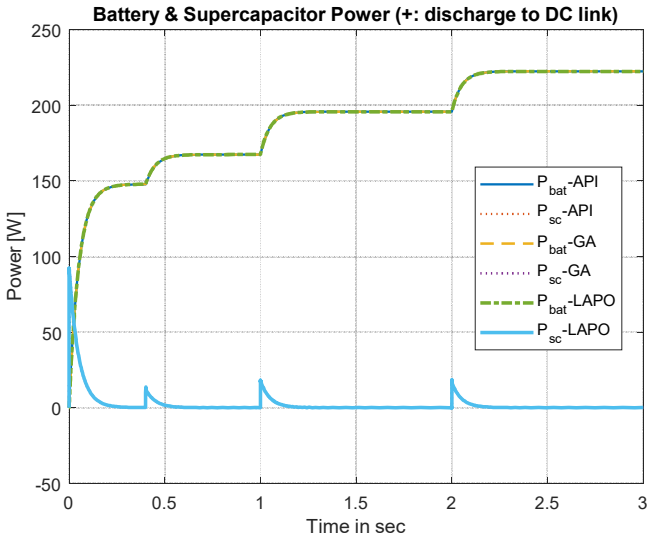

Fig. 15. The output power participation of the hybrid battery-SC during solar irradiance and temperature variation.

In Table VI, the comparative analysis of the DC-link voltage control parameters indicates that although both the LAPO-PI and GA-PI controllers perform well under fixed operating conditions, their performance degrades when exposed to changes in the environment. The API controller is ideal for off-grid PV systems that are subject to changing irradiance and temperature because it achieves a lower ITAE and robust DC-link voltage regulation through gain adaptation, outperforming offline optimization approaches.

TABLE VI. DC-LINK PI PARAMETERS BASED ON OPTIMIZATION TECHNIQUES

Parameters and specifications	Optimization techniques		Adaptation
	LAPO	GA	API
K_p	67.8648	0.5377	Adaptive
K_i	56.9063	1.8339	Adaptive
ITAE	8.704	10.3	0.04
Overshoot	0.02336	1.3994	0.079041

B. Load Variation

The major advantage of integrating SCs into energy storage systems is that they quickly meet peak load requirements and considerably stabilize fluctuations. For DC load variations, it is represented as a change in the resistance value to provide insights into the direct impact on the stability of the DC link

under adaptive control and how fast energy storage performs in abnormal conditions, especially when the API controller of the DC link is applied. The DC-link must remain stable with respect to the reference voltage $V_{DC}^{*} = 50$ V, even if the load demand changes, as shown in Figure 16, at 0.75 s, 1.5 s, and 2.25 s.

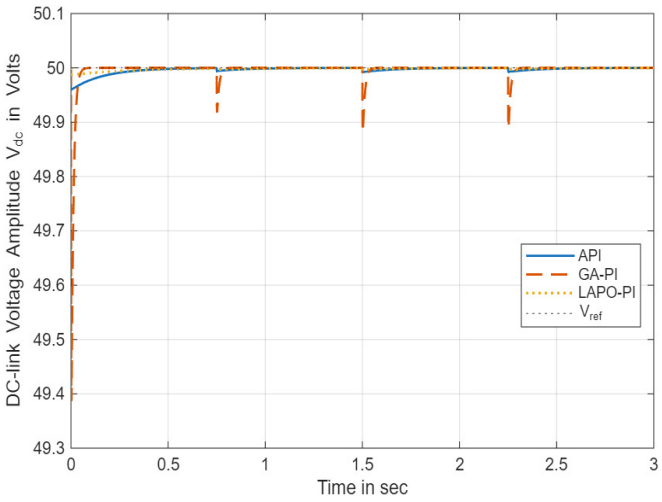

Fig. 16. DC link performance during load variation.

The DC-link-based API controller contributes to better stabilizing the voltage levels and ensures consistent performance regardless of the variations in load demand, as depicted in Figure 16. The dynamic response of the DC-link-based API was faster than that of the DC-link-based optimized PI controllers, such as LAPO and GA. Moreover, it guarantees a lower overshoot. The reason for the increased performance of the API controller is that it depends on self-adaptation to adjust the control parameters.

It has been observed that the battery current rises from a low value to higher levels in response to an increase in load demand. To maintain the battery in good condition, the transitions must be gradual and smooth. In other words, the battery current, as presented in Figure 17, is reduced gradually as the load decreases to prevent stress or abrupt current reversal.

When the load increases, the SC delivers large positive current peaks, rapidly compensating for sudden power demand (Figure 18). During load decrease, the SC absorbs energy, resulting in negative current peaks that help stabilize the DC link voltage. After each transient event, the SC current quickly returns to zero, indicating that it does not participate in a steady-state power supply. The response time of the SC is significantly faster than that of the battery. The SC current, in contrast to the battery current shown in Figure 17, exhibits strong transient peaks in response to changes in load. In Figure 19, the output power of the hybrid battery-SC performed during load variation is similar to that of their respective currents.

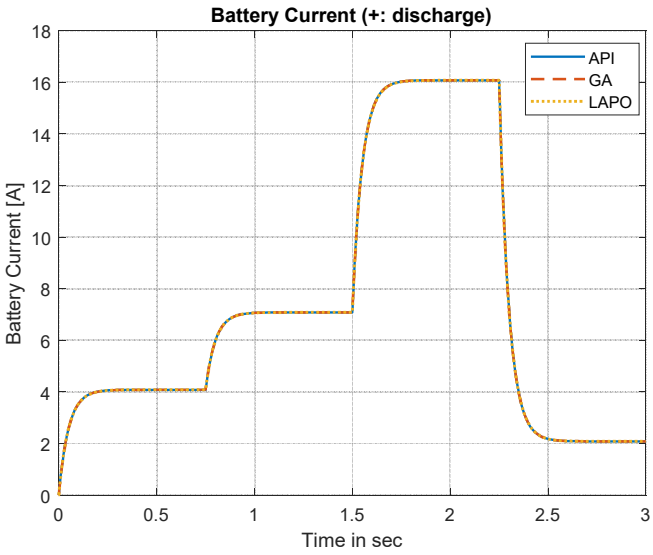

Fig. 17. Battery current.

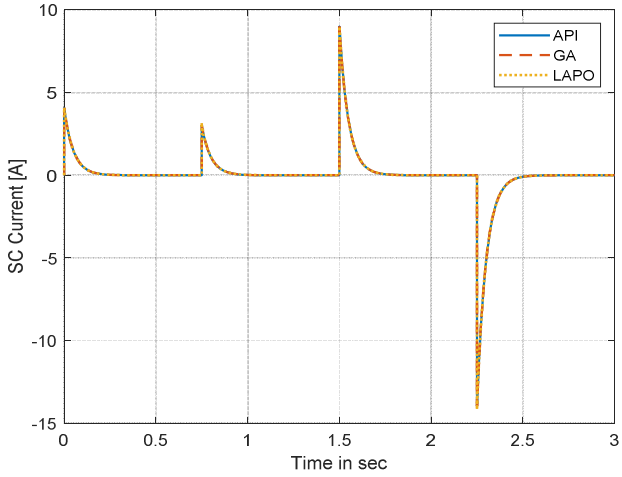

Fig. 18. SC current.

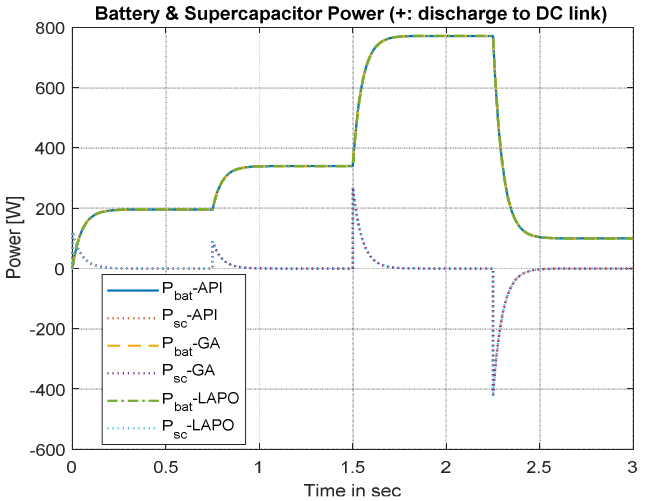

Fig. 19. The output power participation of the hybrid battery-SC during load variation.

For instance, as illustrated in Figure 19, under the load variation test, after 0.75 s, the SC handled the transient, and the battery started discharging energy to supply and meet the load demand. When the load demand increased after 1.5 s, the battery started discharging instantly to meet the high load demand. Conversely, when the load demand further increases at 2.25 s, the battery starts discharging. This frequent load variation affects the battery lifespan; therefore, the SC is incorporated to lessen the burden on the battery. The SoC, shown in Figures 20 and 21, mainly indicates the operating performance of the energy storage system. The SoC in Figure 20 starts at 50% as the initial operating point of the battery. During the 3 s of simulation, the battery started charging, and the battery's SoC gradually increased to almost 50.033% at 1.5 s in the charging phase. At 1.5 s, the SoC reaches a maximum value of 50.033%, and then gradually decreases, indicating that the battery is in the discharging phase due to load variation, reduction in PV power generation, and DC-link voltage support requirement. The SoC profile of the battery reflects small SoC variation, stable power management, and improved battery lifetime, which reduces the stress on the battery.

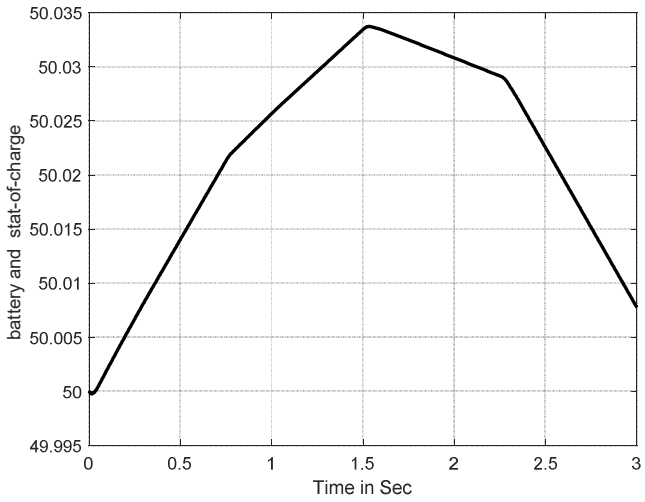

Fig. 20. The SoC of the battery profile.

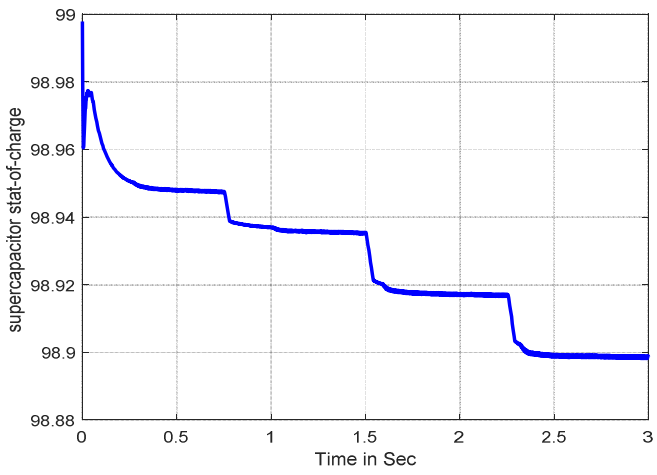

Fig. 21. The SoC of the SC profile.

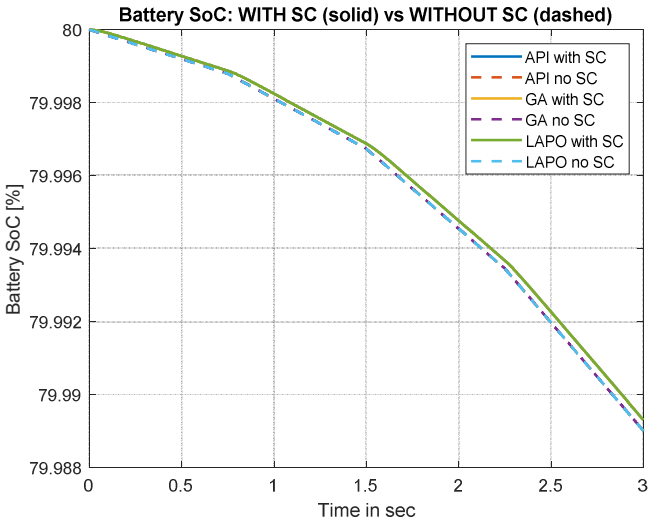

Fig. 22. Battery SoC with and without an SC.

In contrast, as portrayed in Figure 21, the SoC of the SC started at 99%, indicating a full charge, and gradually decreased owing to its high power density, low resistance, and prompt response to DC-link voltage control. In addition, although the SC supplied power by proper power sharing with the battery, its SoC remained above 98.9% owing to the low depth of discharge and operating in a safe operating region. The overall profile assessment for energy storage indicates that the battery is most likely supplying the average power, while the SC is energizing only high-frequency components.

Figure 22 illustrates the results of the battery SoC with and without an SC. Incorporating the SC decreased the battery current across all controllers. The principal method for prolonging battery life is the SC, which absorbs high-frequency current transients, thereby stabilizing the load profile of the battery. However, the SC's value proposition mostly pertains to hardware design rather than control design, as its incorporation yields a modest, although consistent, life extension of approximately 2.77%, irrespective of the controller employed.

The results confirm that the hybrid storage of batteries and SCs effectively separates the transient and steady-state power demands. In other words, the SC alleviates rapid power fluctuations with a negligible depth of discharge, whereas the battery supplies the average power demand with a smooth change in the SoC. This coordinated operation ensures stable DC link voltage regulation, reduced battery stress, and improved system reliability, making the proposed API control strategy highly suitable for off-grid PV system applications.

A stable DC link significantly contributes to controlling the flow of electricity between the PV panel, energy storage, and load, thus ensuring efficient energy distribution. All positive values of the SC and battery were considered discharge events to meet the load demands.

It has been found that solar irradiance and temperature variations mainly affect long-term energy balance and battery state of charge, but load variations put the greatest immediate stress on the energy storage connected to off-grid PV systems

because they affect power balance and DC-link voltage stability. Consequently, changes in the load control the dynamic performance in the short run, while changes in solar irradiance and temperature control the lifetime and use of storage in the long run.

From Table VII, the comparative analysis of the DC-link voltage control parameters under load variation indicates that although the LAPO-PI and GA-PI controllers can maintain the DC-link voltage, their fixed-gain characteristics constrain their robustness. The API controller attains a lower ITAE with minimum overshoot by dynamically adapting control gains, hence assuring enhanced disturbance rejection and stable DC-link voltage regulation during abrupt load variations in off-grid PV systems.

TABLE VII. DC-LINK PI PARAMETERS BASED ON OPTIMIZATION TECHNIQUES

Parameters and specifications	Optimization techniques		Adaptation
	LAPO	GA	API
K_p	341.963	3.320	Adaptive
K_i	772.679	379.443	Adaptive
ITAE	0.01454	0.01354	0.02461
Overshoot	0.07566	7.0223	0.079041

V. CONCLUSIONS

In this study, an Adaptive Proportional-Integral (API) self-tuning controller was employed to regulate the DC link and ensure the safety and continuity of the electricity supplied to the DC load through adaptive hybrid power management. This adaptation of power management, starting from the DC link, managed the power flow from solar PV power generation to load demand, thus fulfilling load demands and maintaining DC link voltage stability within the hybrid energy storage system. Engaging the API controller, which was fed into both the current battery reference and the current Supercapacitor (SC) reference, ensured that the power management prevented the battery from overcharging by compensating the power demand from the SC, thus limiting its degradation and enhancing the overall performance of the off-grid system under two different scenarios, namely solar irradiance and load variation.

DECLARATION OF COMPETING INTERESTS

The author declares no competing interests.

ACKNOWLEDGMENT

The author declares that no external funding was received for this work.

DATA AVAILABILITY

The data presented in this study are available upon request. The data are not publicly available because they are crucial for an ongoing study.

REFERENCES

[1] O. M. Toledo, D. O. Filho, and A. S. A. C. Diniz, "Distributed photovoltaic generation and energy storage systems: A review," *Renewable and Sustainable Energy Reviews*, vol. 14, no. 1, pp. 506–511, Jan. 2010, https://doi.org/10.1016/j.rser.2009.08.007.

[2] W. C. De Carvalho, R. P. Bataglioli, R. A. S. Fernandes, and D. V. Coury, "Fuzzy-based approach for power smoothing of a full-converter wind turbine generator using a supercapacitor energy storage," *Electric Power Systems Research*, vol. 184, July 2020, Art. no. 106287, https://doi.org/10.1016/j.epsr.2020.106287.

[3] J.-K. Lee and J.-R. Yoon, "Effect of Electric Properties according to Volume Ratio of Supercapacitor and Battery Capacitor in Hybrid Energy Storage System," *Coatings*, vol. 13, no. 8, July 2023, Art. no. 1316, https://doi.org/10.3390/coatings13081316.

[4] E. Lim, C. Jo, and J. Lee, "A mini review of designed mesoporous materials for energy-storage applications: from electric double-layer capacitors to hybrid supercapacitors," *Nanoscale*, vol. 8, no. 15, pp. 7827–7833, 2016, https://doi.org/10.1039/C6NR00796A.

[5] A. Lahyani, P. Venet, A. Guermazi, and A. Troudi, "Battery/Supercapacitors Combination in Uninterruptible Power Supply (UPS)," *IEEE Transactions on Power Electronics*, vol. 28, no. 4, pp. 1509–1522, Apr. 2013, https://doi.org/10.1109/TPEL.2012.2210736.

[6] C. Y. Yee, N. Shafiabady, and D. Isa, "Optimal Sizing Supercapacitor-battery Hybrid Energy Storage System in Solar Application using the Genetic Algorithms," *International Journal of Robotics and Mechatronics*, vol. 1, no. 1, pp. 44–52, June 2014, https://doi.org/10.21535/ijrm.v1i1.85.

[7] N. Regis, C. M. Muriithi, and L. Ngoo, "Optimal Battery Sizing of a Grid-Connected Residential Photovoltaic System for Cost Minimization using PSO Algorithm," *Engineering, Technology & Applied Science Research*, vol. 9, no. 6, pp. 4905–4911, Dec. 2019, https://doi.org/10.48084/etasr.3094.

[8] H. Liu, X. Liu, S. Wang, H.-K. Liu, and L. Li, "Transition metal based battery-type electrodes in hybrid supercapacitors: A review," *Energy Storage Materials*, vol. 28, pp. 122–145, June 2020, https://doi.org/10.1016/j.ensm.2020.03.003.

[9] A. Afif, S. M. Rahman, A. Tasfiah Azad, J. Zaini, M. A. Islan, and A. K. Azad, "Advanced materials and technologies for hybrid supercapacitors for energy storage – A review," *Journal of Energy Storage*, vol. 25, Oct. 2019, Art. no. 100852, https://doi.org/10.1016/j.est.2019.100852.

[10] S. Koohi-Fayegh and M. A. Rosen, "A review of energy storage types, applications and recent developments," *Journal of Energy Storage*, vol. 27, Feb. 2020, Art. no. 101047, https://doi.org/10.1016/j.est.2019.101047.

[11] Q. Zhang, L. Wang, G. Li, and Y. Liu, "A real-time energy management control strategy for battery and supercapacitor hybrid energy storage systems of pure electric vehicles," *Journal of Energy Storage*, vol. 31, Oct. 2020, Art. no. 101721, https://doi.org/10.1016/j.est.2020.101721.

[12] P. Singh and J. S. Lather, "Power management and control of a grid-independent DC microgrid with hybrid energy storage system," *Sustainable Energy Technologies and Assessments*, vol. 43, Feb. 2021, Art. no. 100924, https://doi.org/10.1016/j.seta.2020.100924.

[13] M. K. Senapati, K. Al Jaafaari, K. Al Hosani, and U. R. Muduli, "Flexible Control Approach for DC Microgrid Oriented Electric Vehicle Charging Station," in *2023 IEEE IAS Global Conference on Renewable Energy and Hydrogen Technologies (GlobConHT)*, Male, Maldives, Mar. 2023, pp. 1–6, https://doi.org/10.1109/GlobConHT56829.2023.10087864.

[14] B. A. Taye and N. B. D. Choudhury, "A new control method of hybrid energy storage system for DC microgrid application," *Energy Storage*, vol. 6, no. 1, Feb. 2024, Art. no. e564, https://doi.org/10.1002/est2.564.

[15] D. Bazargan, B. Bahrani, and S. Filizadeh, "Reduced Capacitance Battery Storage DC-Link Voltage Regulation and Dynamic Improvement Using a Feedforward Control Strategy," *IEEE Transactions on Energy Conversion*, vol. 33, no. 4, pp. 1659–1668, Dec. 2018, https://doi.org/10.1109/TEC.2018.2837627.

[16] Z. Yang, J. Han, X. Zhou, and T. Tang, "DC-Link Voltage Suppression and Dynamic Improvement of Battery Charging and Discharging System with Feedforward Compensation," in *2023 IEEE 14th International Symposium on Power Electronics for Distributed Generation Systems (PEDG)*, Shanghai, China, June 2023, pp. 543–547, https://doi.org/10.1109/PEDG56097.2023.10215112.

[17] N. Eghtedarpour and E. Farjah, "Distributed charge/discharge control of energy storages in a renewable-energy-based DC micro-grid," *IET*

Renewable Power Generation, vol. 8, no. 1, pp. 45–57, Jan. 2014, https://doi.org/10.1049/iet-rpg.2012.0112.

[18] A. Guichi, A. Talha, E. M. Berkouk, and S. Mekhilef, "Energy management and performance evaluation of grid connected PV-battery hybrid system with inherent control scheme," *Sustainable Cities and Society*, vol. 41, pp. 490–504, Aug. 2018, https://doi.org/10.1016/j.scs.2018.05.026.

[19] M. P. Bonkile and V. Ramadesigan, "Power management control strategy using physics-based battery models in standalone PV-battery hybrid systems," *Journal of Energy Storage*, vol. 23, pp. 258–268, June 2019, https://doi.org/10.1016/j.est.2019.03.016.

[20] J. Liu, X. Chen, S. Cao, and H. Yang, "Overview on hybrid solar photovoltaic-electrical energy storage technologies for power supply to buildings," *Energy Conversion and Management*, vol. 187, pp. 103–121, May 2019, https://doi.org/10.1016/j.enconman.2019.02.080.

[21] Y. Y. Chia, L. H. Lee, N. Shafiabady, and D. Isa, "A load predictive energy management system for supercapacitor-battery hybrid energy storage system in solar application using the Support Vector Machine," *Applied Energy*, vol. 137, pp. 588–602, Jan. 2015, https://doi.org/10.1016/j.apenergy.2014.09.026.

[22] S. Chakraborty, G. Modi, and B. Singh, "A Cost Optimized-Reliable-Resilient-Realtime- Rule-Based Energy Management Scheme for a SPV-BES-Based Microgrid for Smart Building Applications," *IEEE Transactions on Smart Grid*, vol. 14, no. 4, pp. 2572–2581, July 2023, https://doi.org/10.1109/TSG.2022.3232283.

[23] B. A. Taye and N. B. D. Choudhury, "Adaptive filter based method for hybrid energy storage system management in DC microgrid," *e-Prime - Advances in Electrical Engineering, Electronics and Energy*, vol. 5, Sept. 2023, Art. no. 100259, https://doi.org/10.1016/j.prime.2023.100259.

[24] A. G. Khairalla *et al.*, "Enhanced control strategy and energy management for a photovoltaic system with hybrid energy storage based on self-adaptive bonobo optimization," *Frontiers in Energy Research*, vol. 11, Nov. 2023, Art. no. 1283348, https://doi.org/10.3389/fenrg.2023.1283348.

[25] A. Thakur and L. M. Saini, "A voltage and state of charge control technique for battery-supercapacitor hybrid energy storage system for standalone photovoltaic application," in *2015 International Conference on Energy, Power and Environment: Towards Sustainable Growth (ICEPE)*, Shillong, India, June 2015, pp. 1–6, https://doi.org/10.1109/EPETSG.2015.7510142.

[26] A. M. Humada, A. M. Aaref, H. M. Hamada, M. H. Sulaiman, N. Amin, and S. Mekhilef, "Modeling and characterization of a grid-connected photovoltaic system under tropical climate conditions," *Renewable and Sustainable Energy Reviews*, vol. 82, pp. 2094–2105, Feb. 2018, https://doi.org/10.1016/j.rser.2017.08.053.

[27] D. Sera, L. Mathe, T. Kerekes, S. V. Spataru, and R. Teodorescu, "On the Perturb-and-Observe and Incremental Conductance MPPT Methods for PV Systems," *IEEE Journal of Photovoltaics*, vol. 3, no. 3, pp. 1070–1078, July 2013, https://doi.org/10.1109/JPHOTOV.2013.2261118.

[28] X. Dorronsoro, E. Garayalde, U. Iraola, and M. Aizpurua, "Modular battery energy storage system design factors analysis to improve battery-pack reliability," *Journal of Energy Storage*, vol. 54, Oct. 2022, Art. no. 105256, https://doi.org/10.1016/j.est.2022.105256.

[29] S. Kewat, B. Singh, and I. Hussain, "Power management in PV-battery-hydro based standalone microgrid," *IET Renewable Power Generation*, vol. 12, no. 4, pp. 391–398, Mar. 2018, https://doi.org/10.1049/iet-rpg.2017.0566.

[30] R. L. Haupt and S. E. Haupt, *Practical Genetic Algorithms*, 1st ed. Wiley, 2003.

[31] A. Naveed, E. Zerdali, S. Sonmez, and S. Ayasun, "Optimization of PI Controller Gains using Genetic Algorithm for Time-Delayed Load Frequency Control Systems with Electric Vehicles Aggregator," in *2019 11th International Conference on Electrical and Electronics Engineering (ELECO)*, Bursa, Turkey, Nov. 2019, pp. 76–80, https://doi.org/10.23919/ELECO47770.2019.8990434.

[32] D. K. Meena and S. Chahar, "Speed control of DC servo motor using genetic algorithm," in *2017 International Conference on Information, Communication, Instrumentation and Control (ICICIC)*, Indore, India, Aug. 2017, pp. 1–7, https://doi.org/10.1109/ICOMICON.2017.8279122.

[33] P. Bansal and S. S. Gill, "Lightning attachment procedure optimization algorithm for optimal design of digital FIR band stop filter," *Measurement: Sensors*, vol. 24, Dec. 2022, Art. no. 100590, https://doi.org/10.1016/j.measen.2022.100590.

[34] M. Ebeed, A. Ali, M. I. Mosaad, and S. Kamel, "An Improved Lightning Attachment Procedure Optimizer for Optimal Reactive Power Dispatch With Uncertainty in Renewable Energy Resources," *IEEE Access*, vol. 8, pp. 168721–168731, 2020, https://doi.org/10.1109/ACCESS.2020.3022846.

[35] N. G. El Sayed, A. M. Yousef, G. El-Saady, M. D. Alanazi, H. A. Ziedan, and M. Abdelsattar, "Artificial intelligent fuzzy control and LAPO algorithm for enhancement LVRT and power quality of grid connected PV/wind hybrid systems," *Scientific Reports*, vol. 14, Dec. 2024, Art. no. 30475, https://doi.org/10.1038/s41598-024-78384-5.

[36] A. Alhejji and M. I. Mosaad, "Performance enhancement of grid-connected PV systems using adaptive reference PI controller," *Ain Shams Engineering Journal*, vol. 12, no. 1, pp. 541–554, Mar. 2021, https://doi.org/10.1016/j.asej.2020.08.006.